Stepwise Assembly of Tris-Heteroleptic Polypyridyl Complexes of Ruthenium(II)

S. M. Zakeeruddin, Md. K. Nazeeruddin,* R. Humphry-Baker, and M. Grätzel*

Laboratory for Photonics and Interfaces, Institute of Physical Chemistry, Swiss Federal Institute of Technology, CH-1015 Lausanne, Switzerland

V. Shklover

Laboratory of Crystallography, Swiss Federal Institute of Technology, CH-8092 Zürich, Switzerland

Received March 31, 1998

A general method for the synthesis of tris-heteroleptic ruthenium(II) complexes of the type [Ru(dcbpy)(dmbpy)(ddtc)] (**3**) and [Ru(dcbpy)(dmbpy)$(NCS)_2$] (**4**) is reported, where the ligands (dcbpy = 4,4′-dicarboxy-2,2′-bipyridine, dmbpy = 4,4′-dimethyl-2,2′-bipyridine, and ddtc = diethyldithiocarbamate) are introduced sequentially. The complexes have been characterized by UV/visible, emission, IR, Raman and NMR spectroscopies and cyclic voltammetry. The effect of pH on the absorption spectra and luminescence behavior of these complexes consisting of protonatable ligands has been investigated in a water/ethanol solvent mixture by pH titration. The dissociation of protons is in sequential steps (pK_a = 3.5 and 1.8). The excited-state pK_a values are more basic than the ground-state pK_a values. Resonance Raman spectra of these complexes strongly suggest that the lowest-energy metal-to-ligand charge-transfer transition bands are localized on the dcbpy ligand. The molecular crystal structure of **3** and the performance of these complexes as charge-transfer photosensitizers in a nanocrystalline TiO_2-based solar cell is discussed.

Introduction

There is currently considerable interest in ruthenium(II) polypyridyl complexes because of their applications in nanocrystalline TiO_2-based solar cells,[1] biosensors,[2] and molecular wires.[3] The choice of ruthenium metal is of particular interest for a number of reasons: (a) because of its octahedral geometry one can introduce specific ligands in a controlled manner; (b) the photophysical, photochemical, and the electrochemical properties of these complexes can be tuned in a predictable way; and (c) the ruthenium metal possesses stable and accessible oxidation states from I to III.

To introduce different ligands into an octahedral geometry of ruthenium with tailored properties requires a demanding synthetic scheme. There have been few reports on the synthesis and characterization of heteroleptic complexes of ruthenium [Ru$(L^1)(L^2)(L^3)$] starting from a polymeric complex $Ru(CO)_2Cl_2$.[4−6] The synthetic methodology of such heteroleptic complexes involves several steps, resulting in very low yields. Here we have developed a novel synthetic route to introduce different ligands on a ruthenium(II) precursor, i.e., the $RuCl_2(dmso)_4$ complex, which is a versatile and well-characterized starting material. The aim of our synthesis is to explore new pathways for developing efficient charge-transfer sensitizers for nanocrystalline TiO_2 injection solar cells.

The main requirements for such an efficient sensitizer are as follows: (i) large spectral overlap with solar emission spectrum, the optimal threshold wavelength for single-junction quantum converters being around 900 nm; (ii) suitable ground- and excited-state redox properties; and (iii) the presence of interlocking groups for grafting the dye on the semiconductor surface as well as to ascertain intimate electronic coupling between its excited-state wave function and the conduction band manifold of the semiconductor. Toward this end we have engineered Ru(II) complexes at the molecular level to incorporate three different ligands in the same complex. These are judiciously selected to reconcile the tasks of the sensitizer to afford efficient solar light harvesting and vectorial electron injection into the semiconductor. The present study reports the synthesis and characterization of such new sensitizers using a novel synthetic route.

Experimental Section

Materials. The solvents (puriss grade), the ligands 4,4′-dimethyl-2,2′-bipyridine (dmbpy), sodium diethyldithiocarbamate (Naddtc), and potassium thiocyanate were obtained from Fluka. Hydrated ruthenium trichloride was purchased from Johnson Matthey and used as received.

(1) (a) Grätzel, M. *Platinum Met. Rev.* **1994**, *38* (4), 151. (b) Nazeeruddin, Md. K.; Kay, A.; Rodicio, I.; Humphry-Baker, R.; Müller, E.; Vlachopoulos, N.; Grätzel, M. *J. Am. Chem. Soc.* **1993**, *115*, 6382. (c) Argazzi, R.; Bignozzi, C. A.; Heimer, T. A.; Castellano, F. N.; Meyer, G. J. *Inorg. Chem.* **1994**, *33*, 5741. (d) Murakoshi, K.; Kano, G.; Wada, Y.; Yanagida, S.; Miyazaki, H.; Matsumoto, M.; Murasawa, S. *J. Electroanal. Chem.* **1995**, *396*, 27.

(2) Zakeeruddin, S. M.; Fraser, D. M.; Nazeeruddin, M. K.; Grätzel, M. *J. Electroanal. Chem.* **1992**, *337*, 2536. Fraser, D. M.; Zakeeruddin, S. M.; Grätzel, M. *J. Electroanal. Chem.* **1993**, *359*, 125.

(3) Grosshenny, V.; Harriman, A.; Hissler, M.; Ziessel, R. *Platinum Met. Rev.* **1996**, *40*, 72.

(4) Black, D. St. C.; Deacon, G. B.; Thomas, N. C. *Inorg. Chim. Acta* **1982**, *65*, L75−L76.

(5) (a) Anderson, P. A.; Strouse, G. F.; Treadway, J. A.; Keene, F. R.; Meyer, T. J. *Inorg. Chem.* **1994**, *33*, 3863. Anderson, P. A.; Deacon, G. B.; Haarmann, K. H.; Keene, F. R.; Meyer, T. J.; Reitsma, D. A.; Skelton, B. W.; Strouse, G. F.; Thomas, N. C.; Treadway, J. A.; White, A. H. *Inorg. Chem.* **1995**, *34*, 6145−6157.

(6) Black, D. St. C.; Deacon, G. B.; Thomas, N. C. *Aust. J. Chem.* **1982**, *35*, 2445.

S0020-1669(98)00357-7 CCC: $15.00
Published on Web 09/12/1998

$RuCl_2(dmso)_4$[7] and 4,4′-dicarboxy-2,2′-bipyridine (dcbpy)[8] were synthesized using literature procedures.

Analytical Measurements. UV/visible and fluorescence spectra were recorded in a 1-cm-path length quartz cell on a Cary 5 spectrophotometer and Spex Fluorolog 112 Spectrofluorometer, respectively. Electrochemical data were obtained by cyclic voltammetry in a conventional three-electrode cell with a PAR potentiostat. A platinum bead working electrode, platinum wire auxiliary electrode and saturated silver chloride electrodes were used in a single-compartment cell configuration. Proton and ^{13}C NMR spectra were measured on a Bruker 200-MHz spectrometer. The reported chemical shifts were against TMS. Infrared spectra were obtained with a Perkin-Elmer Paragon 1000 FTIR spectrophotometer at a resolution of 5 cm^{-1} with the samples in compressed KBr pellets.

Resonance Raman spectra were measured on a Spex 1877 Triplemate Spectrograph equipped with a Princeton Instruments liquid N_2-cooled CCD-1024E detector. A 1200 groove/mm grating was used, giving a resolution of 2.5 cm^{-1}. Data acquisition was controlled by an Apple Power PC computer running Wavemetrics software to control the PI ST-135 controller and the DM 3000 controller. All the data were corrected for the spectral response of the instrument using a National Bureau of Standards light standard. A coherent Innova 200K Kr^+ laser provided the excitation source. Aqueous solutions of typically 0.5 mM concentration were measured in 1-mm-i.d. capillaries, using a 90° scattering geometry.

Synthesis of $[Ru(L^1)Cl_2(dmso)_2]$ (1; L^1= 4,4′-Dimethyl-2,2′-bipyridine). $RuCl_2(dmso)_4$ (0.484 g) was dissolved in chloroform (100 cm^3), and to this solution was added (0.184 g) 4,4′-dimethyl-2,2′-bipyridine. The reaction mixture was refluxed under nitrogen for 1 h. After allowing it to cool to (25 °C) room temperature, it was filtered through a sintered (G-4) glass crucible. The filtrate was evaporated completely, and the resulting solid was redissolved in acetone in order to remove unreacted $RuCl_2(dmso)_4$. Precipitation of the complex with diethyl ether resulted a fine orange-yellow solid that was filtered and dried under vacuum (yield 0.414 g, 81%). Anal. Calcd for $C_{16}H_{24}N_2O_2 \cdot Ru \cdot Cl_2 \cdot 2.5H_2O$: C, 34.50; H, 5.24; N, 5.02. Found: C, 34.21; H, 5.09; N, 4.91.

Synthesis of $[Ru(L^1)(L^2)Cl_2]$ (2; L^1 = 4,4′-Dimethyl-2,2′-bipyridine, L^2 = 4,4′-Dicarboxy-2,2′-bipyridine). The synthesis and workup of this reaction was performed under reduced light in order to avoid possible cis−trans isomerization. $Ru(L^1)Cl_2(dmso)_2$ (0.4 g) was dissolved in dimethylformamide (100 cm^3) to which the dcbpy ligand (0.19 g) was added. The reaction flask was wrapped with aluminum foil and refluxed under a nitrogen atmosphere for 4 h. The reaction mixture was cooled to 25 °C and filtered. The filtrate was evaporated to dryness, and the solid was dissolved in methanol and filtered. To this methanolic solution was added diethyl ether in order to precipitate the complex **2**. The crude complex **2** was recrystallized from a methanol, diethyl ether, and petroleum ether mixture. The resulting microcrystalline powder was collected on a sintered glass crucible and dried under vacuum (yield 0.35 g, 75%). Anal. Calcd for $C_{24}H_{20}N_4O_4 \cdot Ru \cdot Cl_2 \cdot 4H_2O$: C, 42.83; H, 4.02; N, 8.32. Found: C, 42.80; H, 3.90; N, 8.22.

Synthesis of $[Ru(L^1)(L^2)(ddtc)]$ (3; L^1 = 4,4′-Dimethyl-2,2′-bipyridine, L^2 = 4,4′-Dicarboxy-2,2′-bipyridine, and ddtc = Diethyldithiocarbamate). $[Ru(L^1)(L^2)Cl_2]$ (0.25 g) was dissolved in 250 cm^3 of 3:1 CH_3OH and 0.1 M NaOH solution, under reduced light. Sodium diethyldithiocarbamate trihydrate (0.12 g) was separately dissolved in 10 cm^3 of water and was added to the reaction flask. The reaction mixture was refluxed for 6 h under nitrogen and cooled to room temperature. The solution was filtered through a sintered glass crucible, and the filtrate was evaporated to dryness. The resulting solid was dissolved in water, and the pH of this solution was lowered to 3 by the addition of dilute (0.05 M) nitric acid. At this pH most of the complex precipitates but the flask was kept in a refrigerator at 0 °C for a further 12 h. The precipitate was collected on a sintered glass crucible, washed three times with water at pH 3.5, and dried under vacuum (0.24 g). The crude complex was purified on a neutral alumina column with 0.01 M NaOH containing methanol as a eluent. The alumina column-purified product was further purified by passing through a Sephadex LH-20 gel column. Anal. Calcd for $C_{29}H_{29}N_5O_4 \cdot Ru \cdot S_2 \cdot 3H_2O$: C, 47.63; H, 4.82; N, 9.57. Found: C, 47.67; H, 4.79; N, 9.59.

Synthesis of $[Ru(L^1)(L^2)(NCS)_2]$ (4; L^1 = 4,4′-Dimethyl-2,2′-bipyridine, L^2 = 4,4′-Dicarboxy-2,2′-bipyridine). KNCS (0.582 g) was dissolved in 3 cm^3 of distilled water and transferred into a three-necked flask. To this solution was added DMF (30 cm^3), and the resultant mixture was then purged with nitrogen for 5 min. $[Ru(L^1)(L^2)Cl_2]$ (0.1 g) was introduced as a solid into the flask under reduced light, followed by another 20 cm^3 of DMF solvent. The flask was covered with aluminum foil and refluxed for 5 h. The reaction mixture was allowed to cool and then filtered through a sintered glass (G4) crucible. The DMF and water solvents were removed using a rotary evaporator under vacuum.

To the resulting viscous liquid was added 10 cm^3 of water. To this aqueous solution was added ∼1 cm^3 of 0.05 M NaOH to give a dark purple-red homogeneous solution. The solution was filtered and the pH lowered to 3 with a 0.5 M HNO_3 or CF_3SO_3H acid solution. The resulting dense precipitate was placed in a refrigerator for 12 h at 0 °C. After allowing it to warm to room temperature, the solid was collected on a sintered glass crucible by suction filtration. It was washed (3 × 20 cm^3) with pH 3.5 water that was acidified with the same acid as used previously and air-dried under vacuum (yield 0.09 g, 83%). The crude complex was purified on a Sephadex LH-20 column using methanol as eluent. Anal. Calcd for $C_{26}H_{20}N_6O_4 \cdot Ru \cdot S_2 \cdot H_2O$: C, 47.02; H, 3.33; N, 12.65. Found: C, 47.23; H, 3.33; N, 12.59.

Synthesis of $[Ru(L^2)_2(ddtc)]$ (5; L^2 = 4,4′-Dicarboxy-2,2′-bipyridine and ddtc = Diethyldithiocarbamate). **5** was synthesized using the procedure described for complex **3**. Anal. Calcd for $C_{29}H_{25}N_5O_8S_2 \cdot Ru \cdot 3H_2O$: C, 43.99; H, 3.94; N, 8.84. Found: C, 43.99; H, 3.95; N, 8.84.

Synthesis of $[Ru(L^2)_2(NCS)_2]$ (6) and $[Ru(L^3)_2(NCS)_2]$ (7; L^2 = 4,4′-Dicarboxy-2,2′-bipyridine and L^3 = 4,4′-Dimethyl-2,2′-bipyridine). These complexes were synthesized using the literature procedure.[1b]

Single-Crystal Diffraction Study of the Complex $[Ru(L^1)(L^2)(ddtc)]$. Crystals of **3** were grown from slow evaporation of a methanolic solution containing complex **3**. The structure refinement results and the atomic coordinates are reported elsewhere.[9] The data collection for the platelike single crystal **3** was performed at 210 K on an Enraf-Nonius CAD-4 diffractometer equipped with a graphite monochromator using Mo Kα radiation (λ = 0.710 73 Å). Low-temperature measurement was performed because the crystals were small and also unstable due to the loss of water of crystallization. Using the $w/2\theta$ scan technique, all reflections in the range $2° < 2\theta < 45.94°$ were collected using CAD-4-EXPRESS software.[10] The index ranges were $-12 < h < 12$, $0 < k < 16$, $-20 < l < 20$. Three standard reflections were measured every 1 h for the intensity control and two standard reflections were checked every 100 reflections for the orientational control.

The intensities were measured with a prescan-determined scan speed to reach the ratio $s(I)/I = 0.03$, the maximum measurement time was 30 s/reflection, individual scan range $\Delta\omega = (1.16 - 1.42 + 0.78 \tan \theta)°$, $\Delta\psi = (3.57 - 4.42 + 1.42 \tan \theta)$ mm. For the absorption correction, $\Delta\psi$ scan of nine reflections with the step $\Delta\psi = 10°$ was performed. The minimum and maximum transmission coefficients were 86.25 and 99.89%, respectively. The structure of **3** was solved by direct methods. In difference Fourier synthesis, it was found that crystal **3** consists of crystallization of water molecules and the composition is $C_{29}H_{30}N_5O_4S_2Ru \cdot H_2O$. The structure was refined by full-matrix least squares with anisotropic displacement parameters for the atoms Ru, S, and O and all atoms of terminal methyl, carboxylate, and dithiocarbamate groups. The H atoms in complex **3** were placed at the idealized

(7) Evans, I. P.; Spencer, A.; Wilkinson, G. *J. Chem. Soc., Dalton Trans.* **1973**, 204.
(8) Nazeeruddin, Md. K.; Kalyanasundaram, K.; Grätzel, M. *Inorg. Synth.* **1997**, *32*, 181.
(9) Shklover, V.; Haibach, T.; Bolliger, B.; Hochstrasser, M.; Erbudak, M.; Nissen, H. U.; Zakeeruddin, S. M.; Nazeeruddin, Md. K.; Gratzel, M. *J. Solid State Chem.* **1997**, *131*, 60.
(10) CAD4-EXPRESS. User Manual; Delft Instruments, X-ray Diffraction, Delft, 1992.

Scheme 1

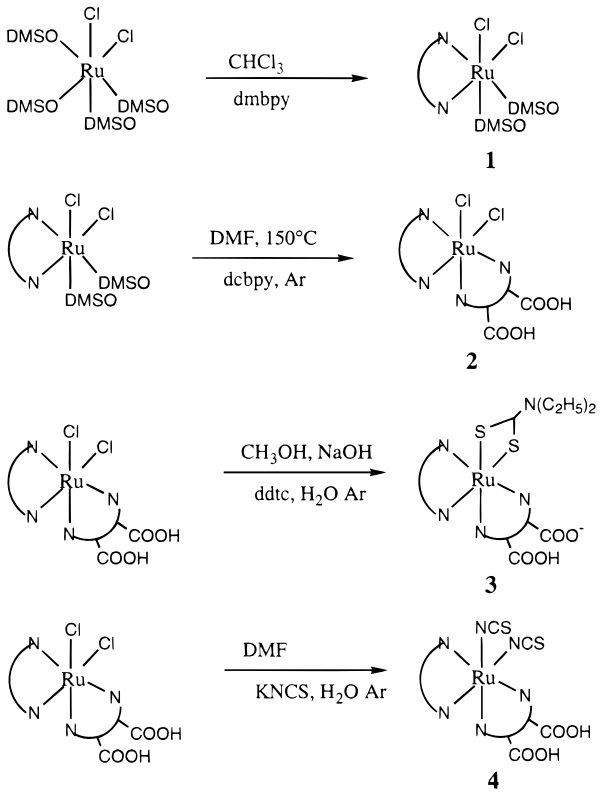

positions and used for the calculation of the structure factors (riding model). The hydrogen atoms of water molecules were not localized.

Photoelectrochemical Measurements. Photoelectrochemical data were obtained using a 450-W xenon light source that was adjusted to give 1000 W/m^2 intensitiy at the surface of the test cell. The spectral output of the lamp was modified with the aid of a Schott KG-5 cutoff filter to reduce the mismatch between the solar simulator and the standard AM 1.5 solar spectral feature in the absorption domain of the sensitizers to less than 2%. The total intensity was routinely checked using a calibrated Si photocell (Laser Components LCE 50).

The photovoltaic output of the solar cells was determined by biasing the cell externally and measuring the generated photocurrent. This process is fully automated by using a National Instruments Lab-NB data acquisition card[11] coupled with Wavemetrics software.[12] A similar system was employed to determine the spectral response of the cell. Again, a 300-W Xe lamp was used, but the light output was focused through a 0.25-m monochromator (PTI) onto the cell under scrutiny. A calibrated photodiode was used to measure the incident photon flux at a given wavelength. In this configuration, the monochromatic light intensity is typically 10−20 W/m^2. The acquisition system measures the photocurrent as it drives the monochromator through a Spex Datascan unit.[13]

Results and Discussion

Scheme 1 shows the details of the synthetic strategy adopted for the synthesis of heteroleptic complexes. Complex **1** was obtained by refluxing $[Ru(Cl)_2(dmso)_4]$ and dmbpy ligand in chloroform. The choice of the solvent is very important in this step. In protic (methanol or ethanol) or high-boiling solvents (dmf, dmso) the reaction leads to a mixture of mono- and bis-complexes. In low-boiling solvent such as dichloromethane, the yields are less than 40%. The ^{1}H NMR spectrum of complex **1** shows six resonance peaks in the aromatic region. The presence of six peaks indicates that the dmbpy ligand is trans to two different ligands. The methyl proton signal in the aliphatic region is observed in the range typical for S-bonded dmso. The reaction of complex **1** with 1 equiv of dcbpy results in the replacement of the remaining two dmso ligands to give complex **2**. The absorption spectrum of complex **2** shows a maximum at 560 nm in ethyl alcohol, which is consistent with the absorption maximums of several known $[RuL_2(Cl)_2]$ complexes.[14] Complexes **3** and **4** were synthesized by substitution of the chloride ligands with diethyldithiocarbamate (ddtc) and NCS^- ligands, respectively.

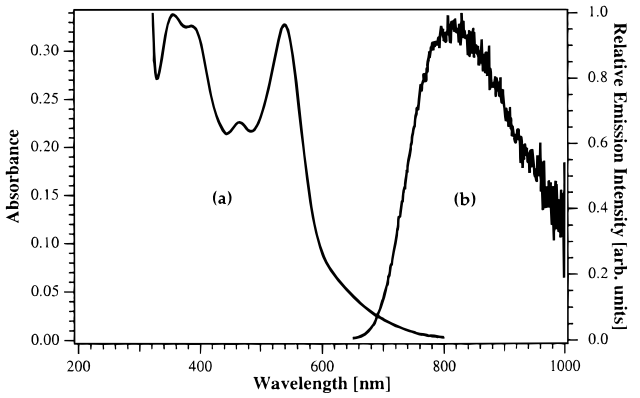

Figure 1. (a) Absorption spectra of complex **3** in ethanolic solution at room temperature. (b) Emission spectrum (λ_{ex} = 550 nm) of complex **3** in ethanolic solution at room temperature.

Electronic Spectra. Complex **3** shows broad and intense visible bands between 390 and 560 nm due to metal-to-ligand charge-transfer transitions (Figure 1a).[15] The low-energy MLCT band of complex **3** is red shifted by 15 nm when compared to the analogous NCS complexes (Table 1). In the UV region, the bands at 290 and 310 nm are assigned to dmbpy and dcbpy ligand $\pi-\pi^*$ charge-transfer transitions, respectively. There are also two distinct shoulders at 390 and 500 nm, which are tentatively attributed to a metal-to-ligand charge-transfer transitions involving the dmbpy ligand. For comparison, the UV/visible spectral data of a homoleptic complex of the type $[Ru(dcbpy)_2(NCS)_2]$ (**6**) were included in Table 1. Complexes **5** and **6** show a band in the UV region at 312 nm that is due to dcbpy ligand $\pi-\pi^*$ charge-transfer transition only.

As discussed above, the ideal sensitizer is black, harvesting the whole range of visible and near-IR light. This can be achieved either by lowering the π^* orbital of the acceptor ligand or by destabilization of the metal t_{2g} orbital. However, a dye having too low a π^* orbital may not be able energetically to inject electrons into the TiO_2 conduction band. In complex **3**, the purpose of introducing the ddtc ligand is to shift the Ru(II) t_{2g} level upward without affecting the π^* level of the dcbpy ligand thereby increasing the MLCT absorption in the red portion of the visible region.

The low-energy absorption maximum of complex **4** is highly solvent sensitive and red shifts 45 nm on going from water (500 nm) to dmso (545 nm), due to the presence of the uncoordinated sulfur atoms. Meyer et al. have observed similar behavior in ruthenium complexes containing CN^- ligands.[16] However, in

(11) National Instruments. http://www.natinst.com/.
(12) Wavemetrics. http://www.wavemetrics.com/.
(13) Instruments S.A. http://www.isainc.com.

(14) Shklover, V.; Nazeeruddin, M. K.; Zakeeruddin, S. M.; Barbe, C.; Kay, A.; Haibach, T.; Steurer, W.; Hermann, R.; Nissen, H.-U.; Grätzel, M. *Chem. Mater.* **1997**, *9*, 430.
(15) Root, M. J.; Sullivan, B. P.; Mayer, T. J.; Deutsch, E. *Inorg. Chem.* **1985**, *24*, 2731.
(16) Timpson, C. J.; Bignozzi, C. A.; Sullivan, B. P.; Kober, E. M.; Meyer, T. J. *J. Phys. Chem.* **1996**, *100*, 2915.

Table 1. Absorption and Luminescence Properties of the Ruthenium Complexes in C_2H_5OH

complex[a]	abs max[b] (nm) ($\epsilon/10^4$ M^{-1} cm^{-1})			Em[c] λ_{max} (nm)	τ/ns at 298 K
	$\pi-\pi^*L^1$	$\pi-\pi^*L^2$	$d\pi-\pi^*$		
$Ru(L^1)(DMSO)_2(Cl)_2$ (**1**)	288 (0.94)		364 (0.21)		
$Ru(L^1)(L^2)(Cl)_2$ (**2**)	296 (3.09)	312 (2.52)	392 (0.92), 546 (0.85)		
$Ru(L^1)(L^2)$(ddtc) (**3**)	295 (3.24)	311 (2.34)	390 (0.98), 541 (1.01)	814	23
$Ru(L^1)(L^2)(NCS)_2$ (**4**)	296 (3.06)	312 (2.41)	385 (1.05), 527 (1.06)	760	37
$Ru(L^2)_2$(ddtc) (**5**)		312 (3.35)	364 (0.97), 548 (1.13)	890	10
$Ru(L^2)_2(NCS)_2$ (**6**)		314 (4.94)	398 (1.31), 538 (1.31)	830	50

[a] L^1 = 4,4′-dimethyl-2,2′-bipyridine, L^2 = 4,4′-dicarboxy-2,2′-bipyridine, ddtc = *N*,*N*′-diethyldithiocarbamate. [b] Values ±2 nm. [c] Measured in ethyl alcohol at room temperature.

complex **3**, under identical conditions the shift in the absorption maximum is only 20 nm.

Emission Spectra. Figure 1b shows the typical emission spectra of complex **3**, obtained by exciting at 550 nm at room temperature in ethanol solution. The emission spectrum of **3** is 54-nm red shifted (Table 1) when compared to complex **4**. The red shift of the emission maximum in complex **3** is consistent with the 14-nm red shift for the lowest metal-to-ligand charge-transfer transition in the absorption spectrum. The RR and electrochemical measurements strongly suggest that the emission occurs from the (dmbpy)(ddtc)Ru^{III}(dcbpy$^-$) charge-transfer excited state.

The emission of these complexes, from the basic form is at higher energy and is more intense as compared with that observed from the acid form. Emission lifetime data are consistent with the trend observed in emission intensities. The red-shifted emission from the protonated form of the complexes is due to stronger π-acceptor properties of the COOH group lowering the energy of the CT excited state. The π^* orbital of the protonated ligand is lower in energy than that of the deprotonated form. The electrochemical data are also consistent with this interpretation. The shorter lived emission lifetime in the acid form of the complexes may arise from proton-induced quenching.

Determination of pK_a. The pK_a's of complex **5** were determined by spectrophotometric titration. A stock solution (5×10^{-5} M) was prepared in 100 cm^3 of an 8:2 H_2O/ethanol mixture containing 0.1 M $NaNO_3$. Since the neutral complex was insoluble in water, 20% ethanol was added in order to avoid precipitation. The initial pH of the solution was adjusted to 11 by adding 0.1 M NaOH solution. The UV/visible spectrum of each solution was obtained after adding acid and allowing the solution to equilibrate for 5 min. The emission spectra were measured at room temperature by exciting into the lowest-energy MLCT band (550 nm).

Complex **5** at pH 11 shows strong visible MLCT bands at 528 and 400 nm, and the high-energy band at 308 nm is due to intraligand transitions of the dcbpy. The ground-state pK_a's can be determined from the relationship between the change in the optical density or the peak maximum with the pH for a given wavelength. When acid is added to an alkaline solution of complex **5**, changes in the electronic spectrum occur as shown in Figure 2a. The MLCT transition band shifts from 528 to 550 nm, upon lowering the pH from 11 to 2, with an isosbestic point at 540 nm. The intraligand transition shifts from 308 to 312 nm with an isosbestic point at 305 nm. The presence of isosbestic points verifies the existence of two species in the equilibrium. Figure 2b shows a titration curve, obtained by plotting the λ_{max} (MLCT) change at 535 nm vs pH for complex **5**. The plot shows the expected sigmoidal shape, with the pH at the inflection point giving the ground-state pK_a value of 3.5 ± 0.1.

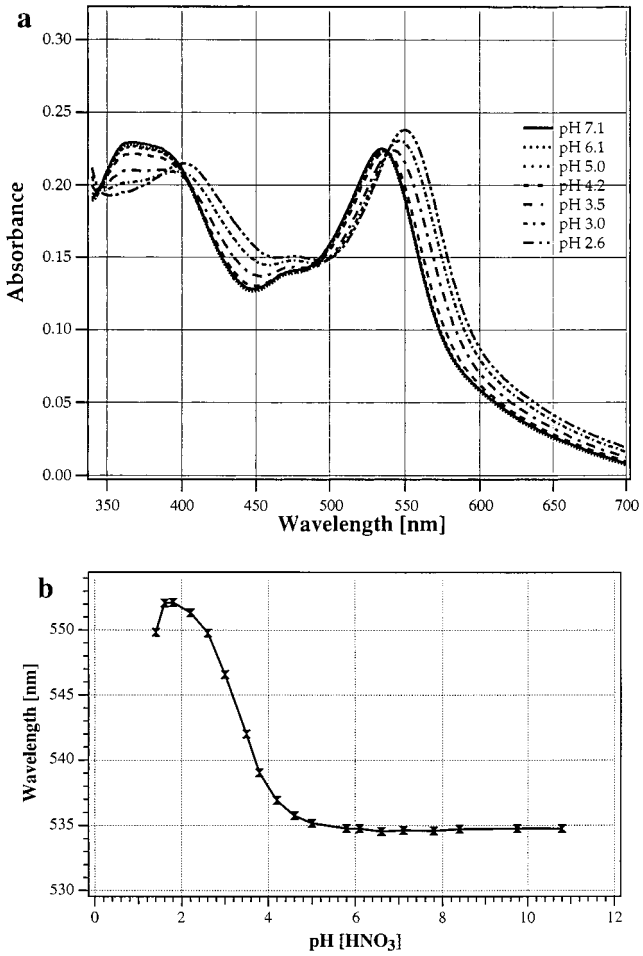

Figure 2. (a) Absorption spectral changes of complex **5** as a function of pH at pH 1 (1), (2) 2, (3) 3, (4) 4, (5) 5, (6) 6, (7) 7, and (8) 8.2. (b) Plot of λ_{max} vs pH for the lowest-energy MLCT band of complex **5**.

Figure 3a shows a titration curve, obtained by plotting the absorbance change at 380 and 310 nm vs pH for complex **5**, in an 8:2 water/ethanol mixture. The 22-nm red shift of the MLCT transition going from basic to acidic pH is due to the protonation of the carboxy groups on the dcbpy ligand.[17] Below pH 4, there are two inflection points at pH 3.5 ± 0.1 and another at pH 1.8 ± 0.1, which we assign to the pK_{a1} and pK_{a2} values of the dcbpy ligand (Scheme 2). The titration of complex **5** in aqueous system shows one inflection at pH 3.2; below pH 2 the complex starts precipitating and we could not determine the second pK_a. The 0.3 pK_a unit difference between aqueous system and mixed-solvent system could be due to the difference in the activity coefficients of the ions.

(17) Giordano, P. J.; Bock, C. R.; Wrighton, M. S. *J. Am. Chem. Soc.* **1978**, *100*, 1170.

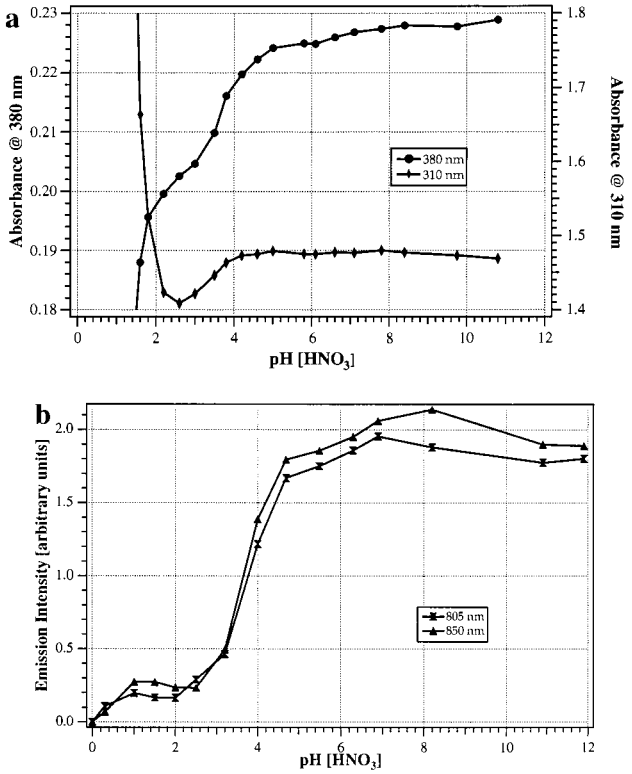

Figure 3. (a) Absorbance at 310 and 380 nm as a function of pH in complex **5**. (b) pH dependence of emission intensity in complex **5**, at ambient temperature in ethanol/H_2O, with excitation wavelength at 530 nm.

Scheme 2

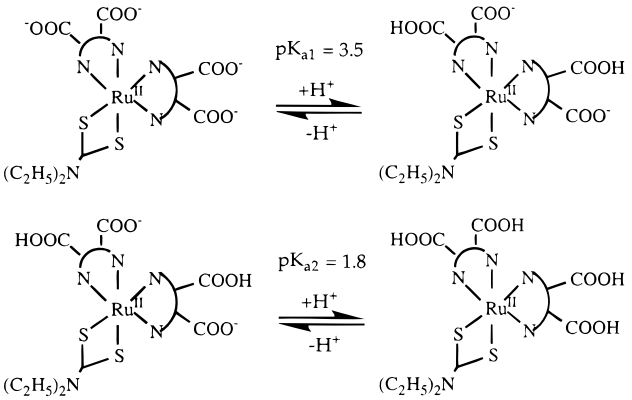

Wrighton et al.[17] investigated the pK_a of the [Ru(bpy)$_2$dcbpy] complex and found only one pK_a at 2.7. Lay and Sasse[18] and Shimidzu and co-workers[19] reinvestigated the acid/base properties of the same complex and found a pK_{a1} at 2.7 and a pK_{a2} below 0.5. In complex **5**, the fact that we see two inflection points at pH 3.5 and pH 1.8 suggests that in this complex the dissociation of the carboxy groups is in a sequential process (Scheme 2). The pK_{a1} of the free ligand is 4.5 and the second one is below 2. The difference between the free ligand pK_{a1} and complex **5** pK_{a1} is 1 unit, which can be considered as a measure of donor strength of the ligand.

It is interesting to compare the ground-state pK_a's of [Ru(dcbpy)$_3$], [Ru(bpy)$_2$(dcbpy)], and complex **5**, which are 2.5, 2.7, and 3.5, respectively. The first pK_a of **5** is 1 pK_a unit more basic than the [Ru(dcbpy)$_3$]. The apparent difference in the pK_a of the dcbpy ligand in complex **5** to that of the tris analogue can be rationalized on the basis of the donor/acceptor properties of dithiocarbamate ligand. The 0.2 pK_a unit difference between the [Ru(dcbpy)$_3$] and [Ru(bpy)$_2$(dcbpy)] is also consistent with the donor strength of bpy compared to the dcbpy ligand. The electrochemical oxidation potential of these complexes decreases in the order [Ru(dcbpy)$_3$] > [Ru(bpy)$_2$(dcbpy)] > [Ru(dcbpy)$_2$(ddtc)]. There is a good correlation between the oxidation potential and the pK_a's of these complexes. The pK_a decreases with increasing Ru(II/III) oxidation potential.

Table 2. Ground-State Redox Potentials of Ruthenium Complexes

complex[a]	oxidation (V vs SCE)	reduction (V vs SCE)
Ru(L^1)(L^2)(Cl)$_2$ (**2**)	0.59	−1.51
Ru(L^1)(L^2)(ddtc)[b] (**3**)	0.67	−1.40, −1.70
Ru(L^1)(L^2)(NCS)$_2$[c] (**4**)	0.78	−1.20
Ru(L^2)$_2$(ddtc)[c] (**5**)	0.80	−1.25
Ru(L^2)$_2$(NCS)$_2$[d] (**6**)	0.85	−1.20

[a] L^1= 4,4′-dimethyl-2,2′-bipyridine, L^2= 4,4′-dicarboxy-2,2′-bipyridine, ddtc = *N*,*N*′-diethyldithiocarbamate. [b] Measured in CH_3CN with 0.1 M tetrabutylammonium tetrafluoroborate. [c] In DMSO. [d] In ethanol.

Figure 3b shows emission intensity at select wavelengths (850 and 805 nm) vs pH in a water/ethanol solvent mixture for complex **5**. The emission spectrum with a maximum at 790 nm in alkaline pH, red shifts to 890 nm, upon lowering of the pH to 2. The emission intensity also decreases with decreasing pH. From spectrofluorometric titration of complex **5**, we were able to estimate the excited-state pK^*_{a1}, which is at 4.0. The 0.5 pK_a unit difference in the ground- and excited-state pK_a of this complex suggests that the ligand electron density is significantly higher in the excited state because of the charge-transfer transition from metal to ligand. In the excited state, the electron is located on the dcbpy ligand and this redistribution of charge creates more electron density on the carboxy groups causing them to be more basic. In a related system [Ru(dcbpy)$_3$], we[20] and others[21] also found that the excited-state pK_a's are more basic than the ground-state pK_a's.

Electrochemical Data. Electrochemical data measured in acetonitrile solvent for complexes **2**−**6** are compiled in Table 2. The cyclic voltammogram of complex **3** shows a quasi-reversible couple at 0.67 V vs SCE with a separation of 80 mV between anodic and cathodic peaks. This we assign to the Ru(II/III) couple. In complex **5**, the Ru(II/III) couple was observed at 0.80 V. For an analogous 2,2′-bipyridineruthenium complex, Meyer et al. reported 0.55 V vs SCE.[15] The difference (0.25 V) in the oxidation potential of complex **5** from that of the 2,2′-bipyridine complex is due to the π-accepting nature of dcbpy. Similarly, the oxidation potential of complexes **4** (110 mV) and **6** (50 mV) are anodically shifted compared to **3** and **5**, respectively. The difference in the oxidation potential between complexes **4** and **3** and **6** and **5** reflects the π-acceptor strength of the thiocyanate ligand compared to the diethyldithiocarbamate ligand.

The oxidation potential in these complexes increases with increase in the π-acceptor strength of anionic ligands, e.g., Cl^- < $ddtc^-$ < NCS^-. The electrochemical data suggest that the chloride and dithiocarbamate ligands are stronger σ/π donors than the thiocyanate ligand. The low-energy MLCT transitions in these complexes are consistent with Ru(II/III) oxidation potentials.

(18) Lay, P. A.; Sasse, W. H. S. *Inorg. Chem.* **1984**, *23*, 4123.
(19) Shimidzu, T.; Iyoda, T.; Izaki, K. *J. Phys. Chem.* **1985**, *89*, 642.
(20) Nazeeruddin, M. K.; Kalyanasundaram, K. *Inorg. Chem.* **1989**, *28*, 4251.
(21) Foreman, T. K. Ph.D. Dessertation, University of North Carolina, Chapel Hill, NC, 1982.

Table 3. ^{1}H NMR Spectral Data of Ruthenium Complexes in Alkaline D_2O

	4,4′-CO_2H bpy						4,4′-CH_3 bpy								Et_2dtc	
complex	H(6)	(H6′)	(H3)	(H3′)	(H5)	(H5′)	(H6)	(H6′)	(H3)	(H3′)	(H5)	(H5′)	CH_3	CH_3′	CH_2	CH_3
3[a]	9.51 (d)	7.91 (d)	8.49 (s)	8.37 (s)	7.63 (d)	7.08 (d)	9.82 (d)	8.17 (d)	9.02 (s)	8.92 (s)	7.63 (d)	7.52 (d)	2.70 (s)	2.47 (s)	3.80 (q)	1.26 (t)
4[b]	9.28 (d)	7.66 (d)	8.45 (s)	8.29 (s)	7.68 (d)	7.04 (d)	9.50 (d)	8.20 (d)	8.98 (s)	8.83 (s)	7.64 (d)	7.36 (d)	2.75 (s)	2.50 (s)		
5	9.57 (d)	7.98 (d)	8.80 (s)	8.66 (s)	7.70 (d)	7.37 (d)									3.80 (q)	1.20 (t)
6	9.55 (d)	7.82 (d)	8.94 (s)	8.77 (s)	8.22 (d)	7.52 (d)										

[a] CD_3OD. [b] Alkaline CD_3OD.

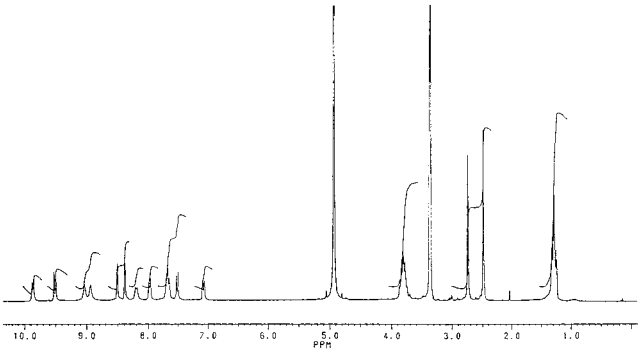

Figure 4. ^{1}H NMR spectrum of complex **3** in 0.05 M NaOD.

There are two quasi-reversible waves in complex **3** at −1.40 and −1.70 V vs SCE that we assign to the reduction of dcbpy and dmbpy ligands, respectively. Complex **5** shows a quasi-reversible wave at −1.25 V, which we assign to the reduction of the dcbpy ligand. The 0.15-V difference in the first reduction potential of complex **3** compared to complex **5** is consistent with the anodically shifted oxidation potential of complex **5**. The electrochemical measurements of these complexes show that the LUMO of the 4,4′-dimethyl-2,2′-bipyridine is higher than the 4,4′-dicarboxy-2,2′-bipyridine. Therefore, in the excited state the electron is transferred to the 4,4′-dicarboxy-2,2′-bpy ligand.

^{1}H NMR Spectral Data. In tris-heteroleptic complexes, the symmetry is lowered to C_1 when compared to homoleptic complexes (D_3). Hence, the NMR spectrum of tris-heteroleptic complexes is expected to be much more complicated.[22] In complexes **3** and **4**, two halves of each ligand are necessarily in different magnetic environments. The NMR spectrum of **3** and **4** in the aromatic region shows 12 resonance peaks and in the aliphatic region two methyl resonance peaks corresponding to two different methyl groups of 4,4′-dimethyl-2,2′-bipyridine. The coordination-induced chemical shifts of methyl protons of 4,4′-dimethyl-2,2′-bipyridine were attributed to the donor nature of the ligand. The apparent difference in the 4- and 4′-methyl protons is due to the trans effect.

In the aromatic region of complex **3**, there are 12 well-resolved resonance peaks corresponding to four different aromatic ring protons of two bipyridines (Figure 4). Table 3 shows the tentative assignments of the various peaks. These assignments are purely based on the positions of the homoleptic complexes. It is interesting to note that there is an asymmetry even in the ethyl protons of coordinated diethyldithiocarbamate ligand in complex **3**. The crystal structure of complex **3** also shows asymmetry in the ethyl groups and is discussed in detail in the crystal structure section.

^{13}C NMR Spectra. Carbon 13 NMR of **4** is useful to identify the mode of coordination of the thiocyanate ligand. The N-coordinated thiocyanate carbon resonance peak has been reported in a number of complexes at 129−135 ppm.[23] In complexes **4** and **6**, the single peak at 133 ppm is due to the N-coordinated thiocyanate ligand. In the aromatic region (δ 170−120 ppm), complexes **3** and **4** show 22 resonance signals corresponding to 22 carbons of dmbpy and dcbpy ligands, whereas complexes **5** and **6** exhibit only 12 resonance peaks coming from two dcbpy ligands. In the aliphatic region, complex **3** shows a broad peak at δ 12.55 and a doublet at δ 45.14 ppm, which are due to the asymmetric methyl and methylene carbon resonance signals of ddtc ligand, respectively. The two peaks at δ 21.13 and 20.95 are due to the asymmetric methyl carbons of dmbpy ligand.

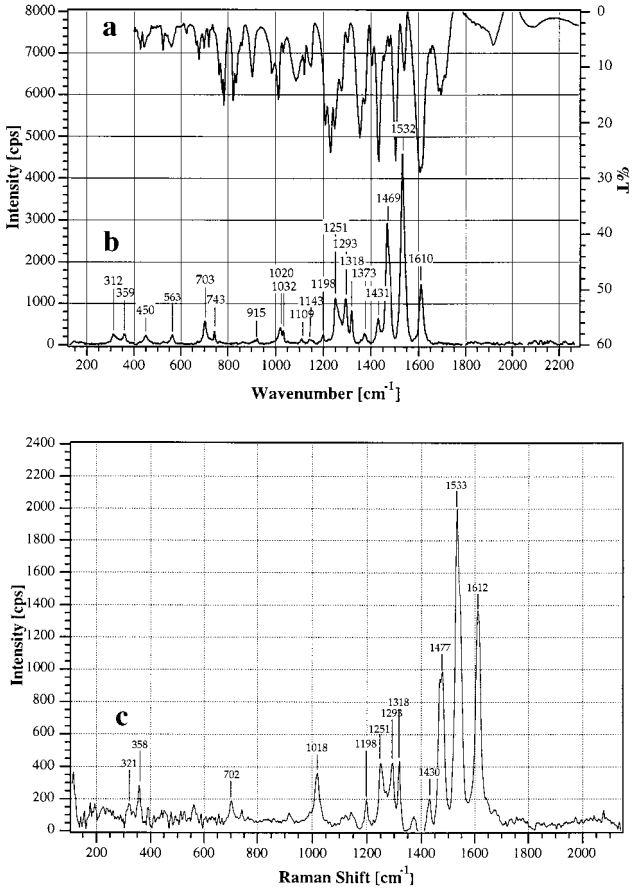

Figure 5. FTIR (a) and resonance Raman (b) spectra of complex **3**, at 530.9-nm wavelength excitation in aqueous solution. (c) Resonance Raman spectra of complex **3**, at 468 nm excitation in aqueous in aqueous solution.

Resonance Raman and IR Spectral Studies. Figure 5 shows the IR and resonance Raman (RR) vibrational spectra of complex **3** for the region 200−2150 cm^{-1}. The IR spectrum is typically complex for a molecule of this size. Nevertheless several diagnostic features are evident as tabulated in Table 4. The carbonyl peaks at 1610 and 1687 cm^{-1} give evidence for

(22) Orellana, G.; Alvarez-ibarra, C.; Santoro, J. *Inorg. Chem.* **1988**, *27*, 1025.

(23) Kohle, O.; Ruile, S.; Grätzel, M. *Inorg. Chem.* **1996**, *35*, 4779.

Table 4. Resonance-Raman and FTIR Spectroscopic Data (cm^{-1}) for Complexes **3** and **5**

	5 (RR)	**3** (FTIR)	**3** (RR)	**3** (calcd)
−CH stretch		2975		2853
$-CH_3$ stretch		2929		2772
$>CH_2$ stretch				2745
$>CH_2$ stretch		2866		2673
>C═O stretch		1687		1770
$n CO_2^-$ (asym)		1610		
ring mode A_1	1612.8		1610.1	1609
		1606		
		1539		
ring mode A_1	1536.7		1532.4	1544
		1504		
ring mode A_1	1472.8		1468.6	1444
−SC═N<	1433		1431	1430
$>CO_2^-$ (sym)	1377		1373	1389
	1296		1318	1299
	1267		1293	1277
	1253		1251	1243
	1145		1143	1174
	1111		1109	
ring breathing	1034		1032	1064
	1021		1020	1052
				883
in-plane bend	705		703	686
				644
			563	558
Ru−S−	453		450	413
Ru−N<	357		359	355
Ru−N<	301		312	321

both the COOH and COO^- functionalities. The numerous ring modes are apparent for both the dcbpy and dmbpy ligands; however, the RR spectrum is contrastingly simpler. This is because the RR intensity is derived from electronic transitions with enhancements occurring in particular for bands having a change in equilibrium displacement between the ground and excited states. Excitation into an allowed MLCT gives rise to resonance enhancements of the symmetric stretching A_1 modes of that ligand only.[24,25] The observed spectral fingerprint is consistent with an effective C_{2V} symmetry. Generally, the A_1 modes have very weak intensities in the IR.

From the broad visible absorption spectrum of complex **3**, several overlapping MLCT transitions are possible, dictated by the energy of the π^* energy level of either the dmbpy or dcbpy ligands. The relative contribution of each transition can be ascertained by examining the resonant enhancement for the A_1 vibrational modes of the different ligands as a function of the probing Raman wavelength. Other groups have demonstrated the utility of this method to map out the MLCT chromophores.[26]

By selecting a wavelength at 530.9 nm, close to the maximum at 530 nm, RR shows a spectrum (Figure 5b) whose marker bands in terms of peak positions are dominated by the Raman bands characteristic of the dcbpy ligand. The quality of the RR data enables the A_1 peaks to be identified by (1) comparison with the RR spectra of analogous homoleptic complexes and (2) calculation using semiempirical methods.[27] The spectral region that is most useful for the characterization of the ligand from 1000 to 1700 cm^{-1} can be seen in Figure 5 and Table 4. The Raman-active modes in this region can be considered as marker bands for the dcbpy ligand in basic aqueous conditions.

Table 5. Experimental Details of the X-ray Structure Determination of the Crystal **3**

chemical formula	$C_{29}H_{30}N_5O_4S_2Ru \cdot H_2O$
formula weight	691.3
crystal color, habit	brown, plate
crystal dimensions (mm)	$0.1 \times 0.2 \times 0.3$
crystal system	monoclinic
lattice parameters	
a (Å)	11.400(4)
b (Å)	15.236(6)
c (Å)	18.748(7)
g (deg)	85.17(3)
V ($Å^3$)	3245(1)
space group	$P2_1/b$
Z	4
density calc (mg/m^{-3})	1.415
absorption coeff (Mo Kα) (mm^{-1})	0.655
F(000)	1428
T (K)	293

In this localized model, the vibrational spectrum is composed of 69 fundamental modes due to the 25-atom framework for the dcbpy ligand. This yields some 24 Raman-active A_1 modes, 3 of which involve the C−H stretch modes, and a further 11 skeletal modes in the 1700−1000-cm^{-1} region. The RR spectrum of **3** at 530.9-nm excitation is nearly identical to the RR spectrum of **5**, supporting the localized description for the excited state of **3** (Table 4).

The second pyridyl-based ligand is used for tuning of the absorption spectrum by modifying the metal-centered orbitals as a function of the electron-donating ability of these ligands. In this case, it is the dmbpy ligand of **3** that is expected to have a higher π^* energy level. Excitation at shorter wavelengths (468 nm) shows that the overall peak intensities are reduced by about half, but in particular the new peaks at 1612, 1545 sh, 1477, and 1318 cm^{-1} become apparent, which are indicative of the dmbpy (Figure 5c). The observed new peak positions are consistent with the RR spectrum of analogous homoleptic complex **7**. The assertion is that the electron is localized on the ligand which is the more easily reducible.

X-ray Structure Determination of Complex 3. The crystal data and details of the X-ray structure determination of **3** are given in Table 5. With three different bidentate ligands, the hexacoordinated Ru atom has a distorted octahedral geometry. The geometry of crystal **3** was observed to be similar to the other structurally characterized ruthenium complexes.[14,28] The molecular structure and adopted numbering scheme of the neutral complex **3** is shown in Figure 6a, the relevant bond distances, bond angles, and torsion angles are given in the Table 6. The Ru−S distances, 2.376 and 2.383(6) Å, are somewhat shorter than in the complex $[Ru(C_3H_6NS_2)(C_5H_5)(C_{18}H_{15}P)]$ (2.394 and 2.397(3) Å).[29] It is interesting to note the SRuN bond angles around the Ru atom, which varies from 91.8 to 96.0(5)°. The different values of bond angles S(1)RuN(4) and S(2)RuN(4) of 95.3(5) and 91.8(5)° may be explained by the different values of the intramolecular contacts C(45)···S(1) and C(45)···S(2) of 3.28(2) and 3.71(2) Å, respectively (Figure 6b). Despite the short C(45)···S(1) contact, the moiety RuS(1)S(2)C(1)N(5) C(2)C(3) remains planar, with a maximum deviation of 0.08 Å. This indicates the existence of a double bond character between the C(1) and N(5) atoms. Nevertheless, some asymmetry still persists in the diethyldithiocarbamate ligand, the S(1)···C(3) and S(1)···C(5) separations somewhat exceed

(24) McClanahan, S. F.; Dallinger, R. F.; Holler, F. J.; Kincaid, J. R. *J. Am. Chem. Soc.* **1985**, *107*, 4860.
(25) Strommen, D. P.; Mallick, P. K.; Danzer, G. D.; Lumpkin, R. S. *J. Phys. Chem.* **1990**, *94*, 1357.
(26) Tait, C. D.; Macqueen, D. B.; Donohoe, R. J.; DeArmond, M. K.; Hanck, K. W.; Wertz, D. W. *J. Phys. Chem.* **1986**, *90*, 1766.
(27) MacSpartan Plus 1.1.6, Wavefunction, Inc., Irvine, CA.
(28) Zakeeruddin, S. M.; Nazeeruddin, M. K.; Pechy, P.; Rotzinger, F. P.; Humphry-Baker, R.; Kalyanasundaram, K.; Grätzel, M.; Shklover, V.; Haibach, T. *Inorg. Chem.* **1997**, *36*, 5937.
(29) Cordes, A. W.; Draganjac, M. *Acta Crystallogr.* **1988**, *C44*, 363.

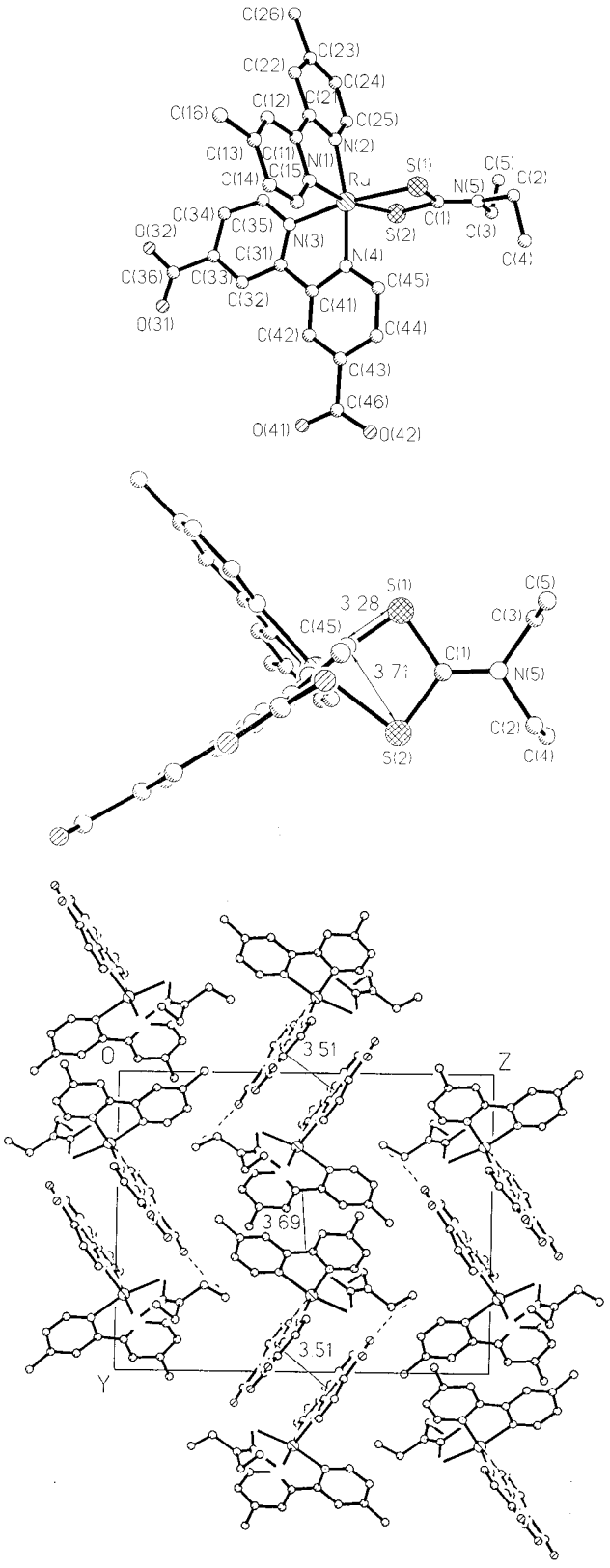

Figure 6. (a, top) Molecular structure and adopted numbering scheme of complex **3**. (b, middle) "Chemical" distortions. Difference between torsion angles in ethyl groups is shown. (c, bottom) Projection of molecular structure of **3** on the plane of the ddtc side shows the asymmetrical orientation of dcbpy ligand in relation to the Ru ddtc cycle.

the corresponding S(2)···C(2) and S(2)···C(4) distances (3.05 and 3.60(2) Å; 3.10 and 3.71(2) Å, respectively).

Table 6. Bond Distances (Å), Angles (deg), and Relevant Torsion Angles (deg) around the Ru Atom in Complex **3**

Bond Distances			
Ru(1)−S(1)	2.376(6)	Ru(1)−S(2)	2.383(7)
Ru(1)−N(1)	2.0782)	Ru(1)−N(4)	2.02(2)
Ru(1)−N(3)	2.07(2)		
Bond Angles			
S(1)−Ru(1)S(2)	72.6(2)	S(2)−Ru(1)−N(4)	91.8(5)
S(1)−Ru(1)−N(1)	96.0(5)	N(1)−Ru(1)−N(2)	79.46(7)
S(1)−Ru(1)−N(2)	93.4(5)	N(1)−Ru(1)−N(3)	88.7(7)
S(1)−Ru(1)−N(3)	171.4(5)	N(1)−Ru(1)−N(4)	95.4(7)
S(2)−Ru(1)−N(4)	95.3(5)	N(2)−Ru(1)−N(3)	94.6(7)
S(2)−Ru(1)−N(1)	167.1(5)	N(2)−Ru(1)−N(4)	170.3(7)
S(2)−Ru(1)−N(2)	94.9(6)	N(3)−Ru(1)−N(4)	77.07
S(2)−Ru(1)−N(3)	103.4(5)		
Torsion Angles			
N(1)−C(11)−C(21)−N(2)	178.2	N(3)−C(31)−C(41)−N(4)	4.2
N(3)−C(31)−C(41)−N(4)	4.2	C(32)−C(33)−C(36)−O(31)	0.4
C(1)−N(9)−C(4)−C(6)	99.2	C(32)−C(33)−C(36)−O(32)	174.1
C(1)−N(9)−C(3)−C(5)	80.2	C(42)−C(43)−C(46)−O(41)	−4.4
N(1)−C(11)−C(21)−N(2)	−1.1	C(42)−C(43)−C(46)−O(42)	175.1

Table 7. Intermolecular Contacts (Å) of Non-Hydrogen Atoms in the Crystal Structure **3**[a] and Characteristic Bond Angles in the Possible Hydrogen Bonds

O(31)···O(42) ($x-1, y, z$)	3.20(3)[b]	C(36)−O(31)−O(42)	141.6(8)
		C(46)−O(42)−O(31)	131.4(8)
O(31)···C(4) ($-x, -y, 1-z$)	3.14(5)		
O(32)···O(42)	2.43(3)[b]	C(32)−O(32)−O(42)	120.7(2)
($-x, {}^1/_2-y, z-{}^1/_2$)		O(32)−O(42)−C(46)	131.4(8)
O(32)···C(44) ($x-1, y, z$)	3.09(4)		
O(41)···C(14)	3.20(3)		
($x, y-{}^1/_2, {}^3/_2-z$)			
O(41)···O(1W) ($x, y, z+1$)	2.89(4)[b]	C(46)−O(41)−O(1W)	107.5(8)
O(42)···C(36) ($x+1, y, z$)	3.22(4)		
C(31)···C(42) ($-x, -y, 1-z$)	3.33(3)		
C(35)···C(46) ($-x, -y, 1-z$)	3.29(3)		
O(1W)···C(24) ($-x, -y, -z$)	3.32(4)[b]	O(1W)−C(24)−C(25)	90.1(9)

[a] Table comprises contacts, which are shorter as corresponding sums of van der Waals radii O + C = 3.32 Å and C + C = 3.40 Å.[21] [b] Hydrogen bond.

In solution studies of **3**, the ethyl groups of diethyldithiocarbamate, in the ^{1}H and ^{13}C NMR time scale, are not chemically equivalent. In crystal **3**, there are no specific intermolecular interactions with the lone pair electrons of N(5) atom and the COOH groups, which might have served as the reason for observed nonequivalence of ethyl groups. The shortest contact of N(5) atom with the oxygen atoms N(5)···O(31)($-1, -y, 1-z$) of 3.437 Å excludes such interaction. The nonequivalence of bond angles and bond distances, as shown above, may explain the observed differences in the ethyl groups chemical shifts in the ^{1}H NMR spectrum of complex **3** or it could be due to the double bond nature of the carbon−nitrogen bond (C(1), N(5)) which is hindering the free rotation of ethyl groups around the nitrogen atom. The observed coplanarity of the Ru−S(1) moiety with a carboxy-substituted bpy ligand and the short intramolecular contact S(1)···C(45) of 3.28 Å may indicate some additional noncovalent interaction of lone pairs of S(1) atom with the π system of dcbpy ligand, which in its turn may cause the asymmetry of ethyl substituents of dithiocarbamate ligand.

The π delocalization between the COOH groups and the corresponding bipyridine moieties could be clearly seen from their coplanarity (Table 7); this is essential for the consideration of location and the excited electron transfer into the semiconductor surface. Crystal **3** is built up along the *y*-axis chains of molecule **3**, associated via the intermolecular $\pi-\pi$ interactions of the bpy ligands. The π interaction of the dcbpy ligands proceeds around the inversion center at (0, 0, $^1/_2$), the dmbpy

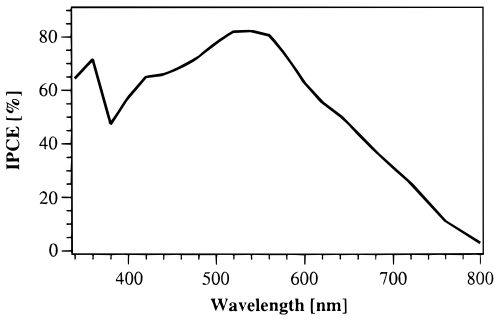

Figure 7. Photocurrent action spectrum for the sensitization of nanocrystalline TiO_2 films by complex **3**. The incident photon-to-current conversion efficiency is plotted as a function of wavelength. A sandwich-type cell configuration was used to measure the spectrum.

ligands interact around the inversion center ($^1/_2$, $^1/_2$, $^1/_2$). In chains, the dcbpy ligands interact more strongly than the dmbpy ligands. The interplanar separations of π systems of bpy ligands are 3.51 and 3.69 Å, respectively (Figure 6c). Similar intramolecular $\pi-\pi$ interactions of bipyridine ligands were found in the crystals of $[(2,2'\text{-bpy})(NCS)]_2Ru(II)$ (solvate with CH_3CN)[30] and $[(4,4'\text{-}(MeO)\text{-}2,2'\text{-bpy})_3Fe(II)(PF_6)_2]$.[31]

The hydrogen bonds between the carboxylate groups (Table 7) contribute to the association of chains of complex **3** into a sheet parallel to the *ab* plane of crystal **3** (Figure 6c). Each molecule within one layer is surrounded by four other mutually centrosymmetrically related antiparallel head-to-tail oriented molecules of **3**. This is in contrast to the tail-to-tail orientation of the neighboring molecules to the *ab* plane of the crystal in which the polar neighboring molecules are oriented in parallel and the outer surfaces are covered by hydrophobic sides of the bipyridine ligands.[28]

Photovoltaic Performance. The performance of **3**−**5** as sensitizers on the nanocrystalline TiO_2 electrode has been studied. The photocurrent action spectra obtained with the TiO_2 films coated with a monolayer of complex **3** is shown in Figure 7. A sandwich-type cell configuration was used to measure the spectrum. The preparation of the nanostructured TiO_2 films and experimental details for the measurements are given earlier.[1b] The dye solutions were prepared in distilled ethanol at a typical concentration of 2×10^{-4} M. The TiO_2 electrodes were heated at 400 °C for 20 min before dipping them into the dye solution. The electrodes were left in the solution for 12−15 h. The redox electrolyte consisted of a solution of 0.6 mM (dimethylpropyl)imidazolium iodide, 100 mM I_2, 0.5 M *tert*-butylpyridine, 100 mM LiI, and 10 mM MgI_2 in methoxypropionitrile.

The incident monochromatic photon-to-current conversion efficiency (IPCE) is plotted as a function of excitation wavelength. The photocurrent action spectrum of complex **3** shows broad features covering a large part of visible spectrum and displays a maximum around 550 nm, where the IPCE exceeds 80% in the presence of deoxycholic acid (cheno) as coadsorbant. However, in the absence of cheno, the IPCE values, which are in the range of 30−50%, are not reproducible. The low IPCE in the absence of cheno could be due to the formation of aggregates on the TiO_2 surface. The aggregation phenomenon could result from hydrogen bonding between the carboxy groups and the lone pair of electrons on the nitrogen of the ddtc ligand or stacking of the bipyridine rings. The crystal structure of complex **3** shows the aggregation is mainly due to the formation of chains along the *y* axis associated with intermolecular $\pi-\pi$ interactions of the bipyridine ligands coupled with hydrogen bond formation between COOH groups.

Conclusions

Tris-heteroleptic complexes of ruthenium were prepared using a novel synthetic route and characterized with respect to their absorption, luminescence, and redox behavior. The determination of the ground-state pK_a's provides evidence for the sequential protonation of the 4,4′-dicarboxy-2,2′-bipyridine. The difference between the free ligand pK_{a1} and the complex **5** pK_{a1} is 1 unit, which can be considered as a measure of donor strength of the ligand. The 0.5 pK_a unit difference in the ground- and excited-state pK_a of this complex suggests that the ligand electron density is significantly higher in the excited state because of charge-transfer transition from metal to ligand. The photocurrent action spectra of these complexes show broad features covering a large part of the visible spectrum and displays a maximum around 550 nm, where the IPCE exceeds 80%. The crystal structure shows the aggregation is mainly due to the formation of chains along the *y* axis associated with intermolecular $\pi-\pi$ interactions of the bipyridine ligands coupled with hydrogen bond formation between COOH groups.

Acknowledgment. We thank to Drs. K. Kalyanasundaram, F. P. Rotzinger, P. Péchy, N. Vlachopoulos, and Marie Jirousek for their help and financial support by a grant from the Swiss Energy Office (OFEN) and the Institut für Angewandte Photovoltaik (INAP), Germany.

IC980357S

(30) Herber, R. H.; Nan, G.; Potenza, J. A.; Schugar, H. J.; Bino, A. *Inorg. Chem.* **1989**, *28*, 938.
(31) Shklover, V.; Nesper, R.; Zakeeruddin, S. M.; Fraser, D. M.; Grätzel, M. *Inorg. Chim. Acta* **1996**, *247*, 237.